

DECOLOURISATION OF EMERGING TEXTILE DYES FROM AQUEOUS SOLUTION USING PNS -NANOCOMPOSITE

S. INDHU, K. MUTHUKUMARAN*

Department of Chemistry, Government College of Technology, Coimbatore-13, Tamil Nadu, India

The objective of this work is to establish the performance of a potential adsorbent from palm-nut shell (PNS), an agricultural low-cost precursor for the removal of acidic dyes- Reactive red 195A (RR195A) and Reactive blue 160 (RB160). The modification of PNS-activated carbon was exhibited by precipitating the magnetite nanoparticles using co-precipitation method resulting in enriched PNS-nanocomposite. The structural morphology of PNS-nanocomposite were characterised by using BET surface area (BET), X-ray diffraction analysis (XRD), Raman spectroscopy (RS), VSM data, High Resolution TEM (TEM) with SAED pattern. TEM pictures showed that the prepared nanocomposite was in pseudo-ball shaped. The microporous and mesoporous pore structures of the adsorbent were known to be obtained by t-plot and BJH respectively. The low retentive force value and saturation magnetisation (0.84 emu) value justify the magnetic separation from the aqueous solution. The best fit of pseudo-second order kinetics model with the high coefficient value better describe the process of adsorption of Reactive red 195A and Reactive blue 160 onto the adsorbent. The monolayer Langmuir isotherm (23.8 mg/g – RR195A & 62.5 mg/g – RB160) pictured the better fit. Thermodynamic parameter values (ΔS_1 , ΔH_1 , ΔG_1) confirm the dependency of temperature by the adsorption reaction process between adsorbent and adsorbate and their spontaneous and endothermic nature was also justified. The result of this work will be useful for future studies in the degradation of azo dyes using affordable precursor PNS. These studies confirm the eligibility of the adsorbents indicating their valuable application such as high adsorption capacity, excellent separation nature in the field of adsorption process for the clean-up of wastewater.

(Received December 1, 2017; Accepted February 3, 2018)

Keywords: Palm nut-shell, Nanocomposite, Reactive dyes, Microporous & Mesoporous structures, TEM analysis

1. Introduction

Dye pollution resulting from vast textile industries and improper discharge of untreated and highly coloured dye effluents [1] into water streams is considered to be a massive hazard lead to the environment [2]. Coloured water stream is highly toxic to all living species depend on them. Their accumulation also causes skin irritation, carcinogenic and eye-deficiency to human beings and affects the aquatic living species in a great manner [3]. According to textile industrialists, reactive dyes are extremely powerful in bonding with the fabric and so with water. Hence in an environmental view, it is highly deleterious substance in the soluble form [4].

The most common ways for the removal of colourants are chemical and biological precipitation. But these were highly dependent on solute concentrations [5]. Among various processes of dye removal, it was justified that adsorption technique would be cost-effective, ease-operative, high efficiency and reliable process [5,6]. Activated carbon (AC), a well known high surface area adsorbent possesses high capability in treating wastewater containing heavy metal ions, organics like dyes, surfactants and soaps etc.,[7]. So researchers find more ways in carbonising and activating the natural precursor for synthesising an effective AC [8]. Nowadays,

*Corresponding author: bamikumar@gct.ac.in

impregnating metal oxides into the AC in the productivity of nanocomposite has made betterment in the adsorption technique. These types of adsorbents also possess relatively more applications in the adsorption technique [5,10]. Their reusable and recoverable properties are easier and so the researchers nowadays prefer this type of nanocomposite [9].

In the proposed study, a suitable precursor palm-nut shell was taken in the production of remarkable AC with high porosity and adsorption properties. This economical AC was further treated to impregnate with magnetite resulting in PNS-nanocomposite. It is fundamental to characterise PNS-nanocomposite to know and describe them better. The characterisation and thermodynamic studies have been attempted to show the eligibility of the adsorbent in the adsorption technique.

2. Experimental Materials

The palm-nut shell an agricultural precursor can be widely found in the nearby vegetation fields. The chemicals procured from Sigma-Aldrich Chemical Company with the analytical grade. The synthetic dyes (Reactive red 195A and Reactive blue 160) were purchased from Jay Chemicals Industries Limited, India.

3. Experimental Methods

3.1 Synthesis of PNS-nanocomposite

Fifty grams of precursor agricultural product was taken, washed several times and dried naturally for about 3 days. The products were crushed into smaller pieces and then these pieces were placed in a porous pot under CO₂ atmosphere. The activation was carried out at above 750 °C for about 10 minutes. The resultant was cooled and again washed with mild acid once and with double distilled water for removal of any impurities [11]. The obtained final product High-Temperature AC derived from the palm-nut shell (PNS-AC).

The simplified co-precipitation method was prevailed to modify PNS-AC as an effective PNS-nanocomposite. PNS-AC derived was taken in the powdered form and orderly it was added with ferrous sulphate solution in the ratio of 1:5 respectively. Then freshly prepared sodium hydroxide was added dropwise to obtain deep green coloured resultant. The resultant was kept aside for better settling. The settled precipitate was sonicated by using ultra sonicator for about 3 cycles. The resulted solution was expected to be iron hydroxides and it was washed with double distilled water and then dried in a hot air oven at 120°C. At this temperature, iron hydroxides were meant to turn out as iron oxides accumulating on PNS-AC in the formation of a black coloured PNS-nanocomposite. The expected formation of magnetite iron oxide in PNS-nanocomposite was confirmed and justified by the values of p-XRD in the forthcoming discussion below.

3.2 Characteristics studies

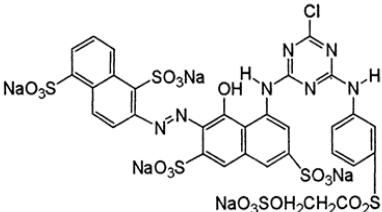
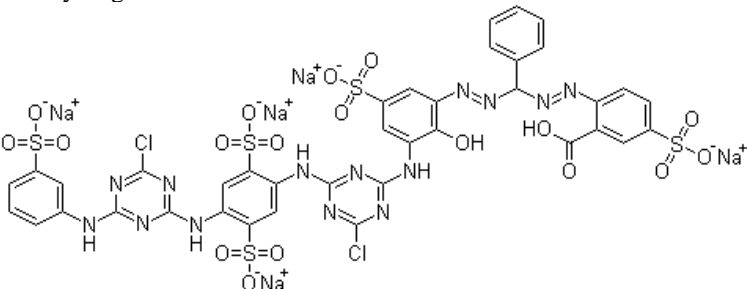
The characteristics such as specific surface area, average pore size and pore volume of PNS-nanocomposite was measured by BET and BJH method of nitrogen isotherms (Micromeritics ASAP 2020). The vibrational sample magnetometer (Lakeshore VSM 7410) was to state the magnetic property of PNS-nanocomposite. The p-XRD analysis results were specific to confirm the formation of magnetite using X'Pert Pro – PAnalytic Powder X-Ray Diffractometer. Raman spectroscopy was employed to identify the functional groups present in the adsorbent. The surface morphology, size and shape of PNS-nanocomposite were well portrayed by using HR-TEM analysis (Jeol/JEM 2100).

3.3 Adsorbate characteristics

Reactive Red 195A (RR195A) (Fig. 1a), pentasulphonatomo azo dye molecule and Reactive Blue 160 (RB160) (Fig. 1b), pentasulphonatodi azo dye molecule was taken for the present investigation. These dyes were now a widely used product of textile industries and contain different characteristic natures in them. Hence in the present work, these were subjected to the

study and their results were compared. The λ_{\max} (wavelength) was determined using standard method and noted in Table 1. The stock solutions were prepared by dissolving exactly 1 g of the synthetic dye in a litre of double distilled water. From the stock, the solutions were diluted for further attempts of the adsorption tests and the final concentration of dye remained in the supernatant solution was measured using Perkin-Elmer UV-VIS spectrophotometer. The details of both the adsorbates were mentioned in Table 1.

Table 1: Adsorbate characteristics

Name of the Dye	Reactive red 195A
λ_{\max}	510 nm
C.I Index	CAS 77365-64-1
Molecular group	mono- azo class
Molecular name	pentasodium 2-[[[8-[[4-chloro-6-[[3-[[2-(sulphonatooxy)ethyl]sulphonyl]phenyl]amino]-1,3,5-triazin-2-yl]amino]-1-hydroxy-3,6-disulphonato-2-naphthyl]azo]naphthalene-1,5-disulphonate
Molecular structure (Fig. 1a)	
Name of the Dye	Reactive Blue 160
λ_{\max}	600 nm
C.I Index	CAS 93921-06-3
Molecular group	Di-azo class
Molecular name	Cuprate(6-), [2-[[[3-[[4-chloro-6-[[4-[[4-chloro-6-[(3-sulfophenyl)amino]-1,3,5-triazin-2-yl]amino]-2,5-disulfophenyl]amino]-1,3,5-triazin-2-yl]amino]-2-hydroxy-5-sulfophenyl]azo]phenylmethyl]azo]-5-sulfobenzoato(8-)-, hexahydrogen
Molecular structure (Fig. 1b)	

3.4 Equilibration Studies

The following studies were performed to better understand the adsorption of RR195A and RB160 by using *PNS*-nanocomposite. The batch optimisation studies such as i) effect of pH, ii) effect of dosage and iii) equilibration time was studied. Kinetic models studied: i) pseudo-first order and ii) pseudo-second order. Isotherm mechanism attempted: i) Langmuir monolayer isotherm model and ii) Freundlich multilayer isotherm model. Thermodynamic parameter studies were also studied and their results were evaluated.

4. Results and discussion

4.1 Characterisation of PNS-nanocomposite

This Brunauer-Emmett-Teller method computes the surface area and the average pore diameter and cumulative pore volume of the adsorbent. These interpretations (Table 2) were determined by N₂ isotherm (adsorption/desorption) in the P/P₀ range at 77 K and the surface area of studied adsorbent (75 m²/g) was noted to be low compared to PNS-AC. This is because of the introduction of pseudo-ball shaped iron oxide particles onto the active pores of PNS-AC. As per the IUPAC notations, the plot of adsorption/desorption (Figure not shown) denote isotherm- type IV expressing the mesoporous nature [4]. The BJH plot obtained evaluates the existence of mesopores on the surface of the PNS-nanocomposite [14]. While the observation of t-plot (Fig. 2) also symbolise the micropore volume (0.04cm³/g) of the adsorbent which made eligible to deal with larger molecule like RR195A and RB160. The pore- size distribution and average pore size is less than 3 nm which confirm the presence of micropores in the adsorbent [19]. Hence microporous and mesoporous nature of PNS-nanocomposite could sustain high adsorptive performance of the dye molecules taken.

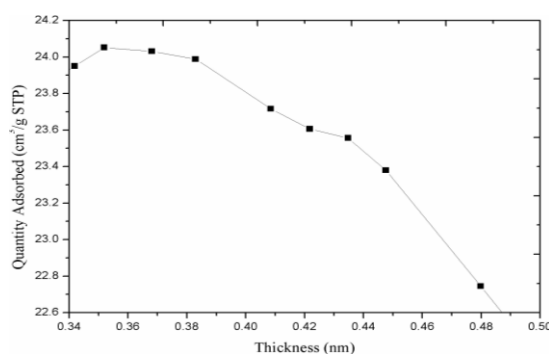


Fig.2.PNS-nanocomposite: t- plot

Table 2.Meso and microstructures and VSM properties of PNS-nanocomposite

	S _{BET} (m ² /g)	V _{pore} (cm ³ /g)	t-plot (cm ³ /g)	Pore width (nm)	Ms (emu/g)	H _{ci} (G)
PNS-nanocomposite	75	0.04	0.04	< 3	0.84	343

The vibrational sample magnetometer was employed to evaluate the magnetic characteristics of PNS-nanocomposite. The response of this VSM study shows a soft hysteresis loop. This analysis was performed at room temperature at ±10KOe.

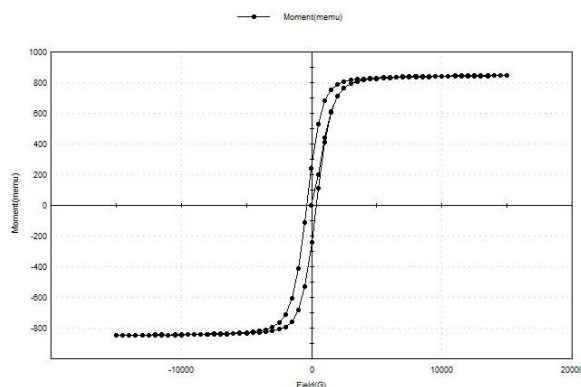


Fig. 3 VSM curve: Magnetic characteristics

The magnetisation value (shown in Table 2) shows the existence of *PNS-AC* precursor. The lower value of retentive force shows the ability to re-dispersion easily in a solution after separation. After manipulating all these points by referring the literature [16] that the value resulted show the strong binding between the native AC and nano magnetite particles.

The hkl values for the corresponding 2θ values were obtained from the suitable JCPDS card (065-3107). The 2θ values of *PNS-nanocomposite* correspond to the miller values 30° (2 2 0), 35° (3 1 1), 43° (4 0 0), 53° (4 2 2), 57° (5 1 1) & 62° (4 4 0) respectively. The observed (Fig. 4) high intense peak values confirm the presence of synthetic magnetite in the form of Fe_3O_4 in the synthesised *PNS-nanocomposite*. As per Scherrer's equation, τ value briefs the adsorbent's grain size (nm). The equation: $\tau = \frac{0.94 \times \lambda}{\beta \times \cos\theta}$, 0.94 = Scherrer constant, $\lambda = 0.154$ nm wavelength of Cu $K\alpha$, $\cos\theta$ = the radian value and β = FWHM value in radians. After substituting the appropriate values, the grain size of the adsorbent was in the range of 3-7 nm.

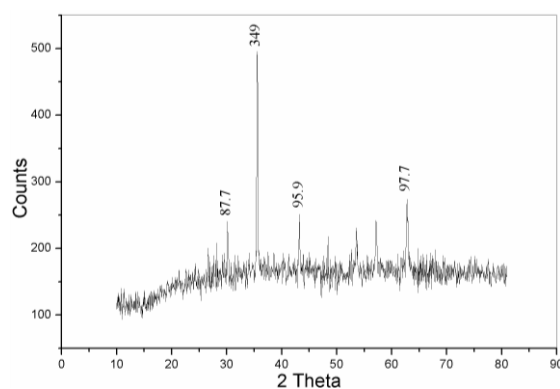


Fig. 4. p-XRD spectra of *PNS-nanocomposite*

From the obtained values of p-XRD analysis, the interpretation was made to confirm the amorphous with high crystallinity structure of the nanocomposite [12].

The Raman spectral data of *PNS-nanocomposite* were observed and shown in Fig.5. The observed spectra expose 259 cm^{-1} (Fe-O symmetric bending), 892 cm^{-1} (Fe-OH asymmetric stretching) and the appearance of D band at 1190 cm^{-1} and G band at 1624 cm^{-1} . These bands furthermore confirm the presence of iron oxide and AC in *PNS-nanocomposite*. [12]. This result further proves the better bonding between iron oxide particles and *PNS-AC* in *PNS-nanocomposite*.

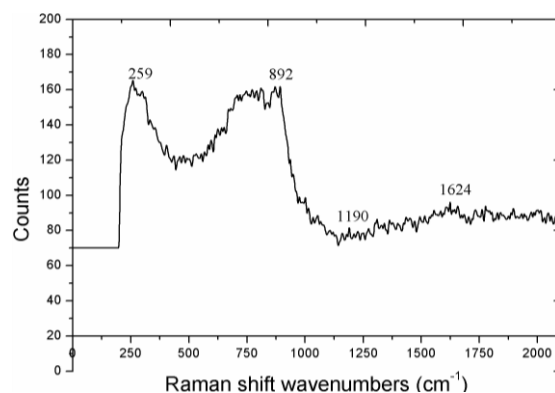


Fig.5. Raman spectra: *PNS-nanocomposite*

The structural properties of *PNS-nanocomposite* were better monitored by HR-TEM analysis. The accumulation of iron oxides onto the activated carbon was observed in the images

obtained. The pseudo-ball shaped magnetite particles enhance the nature of *PNS*-nanocomposite in Fig. 6 a&b. The particle size of *PNS*-nanocomposite was in the size ranges between 1-7 nm. These TEM results also favour the results of p-XRD and the outcome of Scherrer's equation about the grain size of *PNS*-nanocomposite.

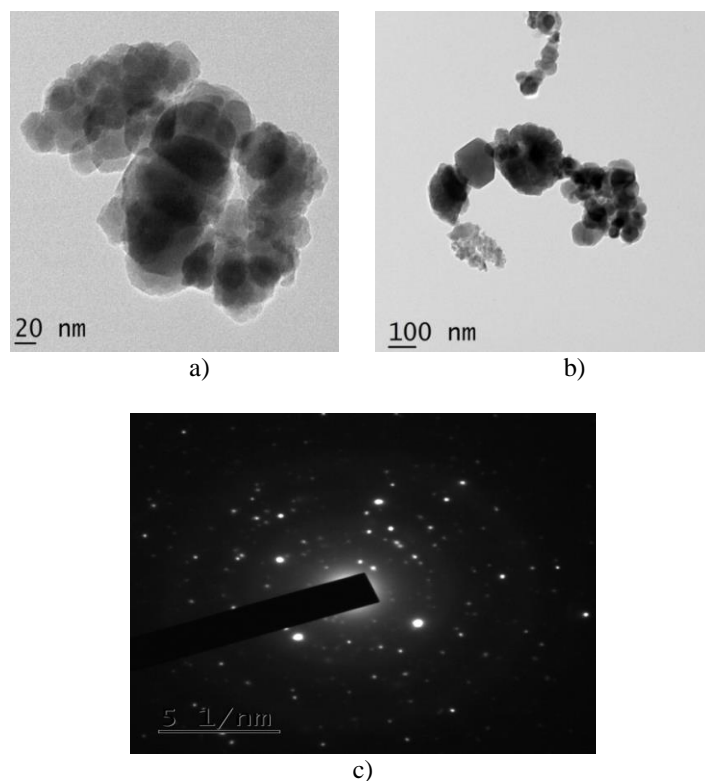


Fig. 6. *PNS*-nanocomposite: a & b) HR-TEM images, c) SAED pattern

The selected area electron diffraction (SAED) pattern depicts the appearance of dull rings and intermittent bright dots (Fig. 6c) that *PNS*-nanocomposite possesses crystallinity in nature [6, 13] as it was already demonstrated by p-XRD analysis data from its hkl peak values.

4.2 Batch optimisation studies

The optimisation studies were carried out and the parameters are the effect of pH, optimum dosage and equilibrium time. The studies were performed using orbital mechanical shaker at the agitation speed of 170 rpm and at room temperature. Equilibration was initiated at a minimum concentration of the dye solution (10 mg/L), 0.1 g dosage and 6 h time initially and after each attempt, the supernatant solution was taken and final concentration of the dye was determined by UV-VIS spectrophotometer. The performance was made individually for each attempted dyes (RR195A and RB160). The amount of dye taken shall be calculated by (equation 1 and 2) [17]

$$\% \text{ Removal of dye adsorbed} = \frac{C_i - C_f}{C_i} \times 100 \quad (1)$$

Amount of dye adsorbed by adsorbate

$$(q_{eq}) = \frac{C_i - C_f}{m} \times V \quad (2)$$

where, C_i = initial concentration of the dye (mg/L); C_f = final concentration of the dye (mg/L); V = volume of the dye solution taken (mL); m = mass of the adsorbent (g)

After pilot testing, the optimisation of pH was made by varying pH from 1 to 10 at room temperature for an extended period of 3h, the optimisation studies were carried out at an

admissible dosage (0.1 g) of *PNS*-nanocomposite. The concentration of the supernatant solution was filtered and the efficiency of the adsorbent at different pH was shown in Fig.7.1. Here in both the cases of dyes, the removal capacity was considerably high (95 % for RR195A and 91% for RB160) in the acidic pH indicating the availability of H^+ ions approaching the negative ions of the dye molecules. And as the pH increases, the concentration of OH^- ions increases and hence the removal capacity was considerably low [17]. The result shows high at pH 4 for RR195A and pH 6 for RB 160, the removal capacity was efficiently high and hence further studies shall be carried out at this optimised value.

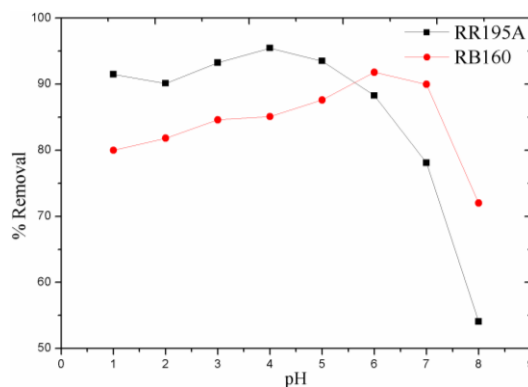


Fig.7.1.pH optimisation

Next, to pH optimisation, the parameter of dose well comprises the removal capacity and utility of the *PNS*-nanocomposite in a better way. The different dosage of adsorbent (0.1 g –1 g) was added to a fixed initial concentration (10 mg/L) of the dye solution and also at optimised pH 4 and pH 6 for RR195A and RB160 respectively and at equilibration time (3 h), the attempts were made. The dye uptake capacity of the adsorbent was considerably high at the initial stage and as the dose increases the availability of active sites also increases for the accumulation of larger dye molecules onto it [18]. Even though selective nature towards azo and sulphonate groups present in the dye molecules were targeted and Fig. 7.2 shows their removal range. The maximum removal (> 90 %) was found in the minimum dosage level itself for both the dyes. As the dosage increases, the uptake of dye molecule also increases and reaches equilibrium [17]. From the obtained values, the adsorbent dosage was optimised as 0.1 g for both the cases of dyes.

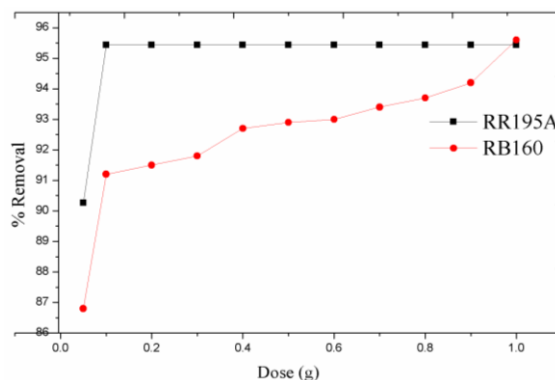


Fig. 7.2 Dosage optimisation

The effect of equilibration time for the *PNS*-nanocomposite adsorbent on the removal of dyes was attempted with a collective sample of known concentration of dye solution at room temperature and at optimised pH and dose, the time interval was varied from 0 to 180 min. It is noted in Figure 7.3, the adsorption of RR195A and RB160 dyes were immediate and reliably high

due to the availability of a larger number of active sites and after attaining the maximum uptake capacity, the reaction attains equilibrium [17]. The maximum uptake (> 90%) of mono-azo class dye (RR195A) was reached at 20 min and the time for RB160 was after 60 min, this is because of the complex structure of latter (di-azo class).

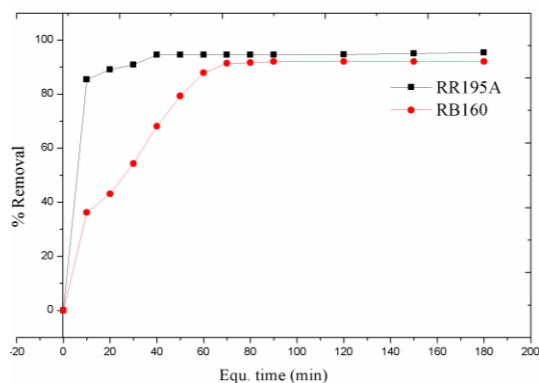


Fig. 7.3 Equi.time optimisation

4.3 Adsorption Kinetic Pattern

The reaction on kinetics gives a sole idea about the interaction time between the adsorbate and adsorbent. The adsorption kinetics describes the rate determining step, operations and feasibility of the process. The pseudo-first order pattern was calculated by the following equation [15],

$$\frac{dq}{dt} = K_i(q_{equ} - q_T) \quad (3)$$

Taking the linear form of the model,

$$\log(q_{equ} - q_T) = \log q_{eq} - \left(\frac{K_i}{2.303}\right)t \quad (4)$$

The experimental value (Table 3) was not favourable to the calculated R^2 and q_{eq} value and this is due to that the process does not depend on only one of the reactant. Hence the adsorption process does not suit the pseudo-first order model.

The pseudo-second order kinetic pattern developed and given as

$$\frac{t}{q_T} = \frac{1}{K_j(q_{eq})^2} + \frac{t}{q_{eq}} \quad (5)$$

where K_j = the pseudo-second order adsorption rate constant, q_T = the amount of dye adsorption at time t . Fig. 8a displays the favour of pseudo-second order model. The dye uptake capacity (q_{equ}) of RR195A was 9.5 mg/g and 9.6 mg/g for RB160. The correlation coefficient for the pseudo-second order model (R^2) was almost equal to unity denoting the better inference of the process between *PNS*-nanocomposite and the dye molecules. The suitability of this kinetic model suggests that the reaction process depends on both the reactants. Based on the values obtained, it can be postulated that, this type of process is all due to the increase in the mobility of dye molecule with temperature rise.

Weber and Morris intra-particle diffusion model proposal was to test the adsorbent and adsorbate

$$q_T = K_p \cdot t_1^{1/2} + C_p \quad (6)$$

where K_p = the rate constant of intra-particle diffusion. The intercept and K_p values are determined from the slope suggesting the linearity of adsorption. According to Eqn. 12 revealing intraparticle diffusion model, the K_p values are determined from the slope and the value of intercept (Fig. 8b) suggests the adsorption was linear and diffusion is greater through the active sites on the nanocomposite. Therefore, the assumption portray that the adsorption onto the surface of the adsorbent and intraparticle diffusion occurs consequently.

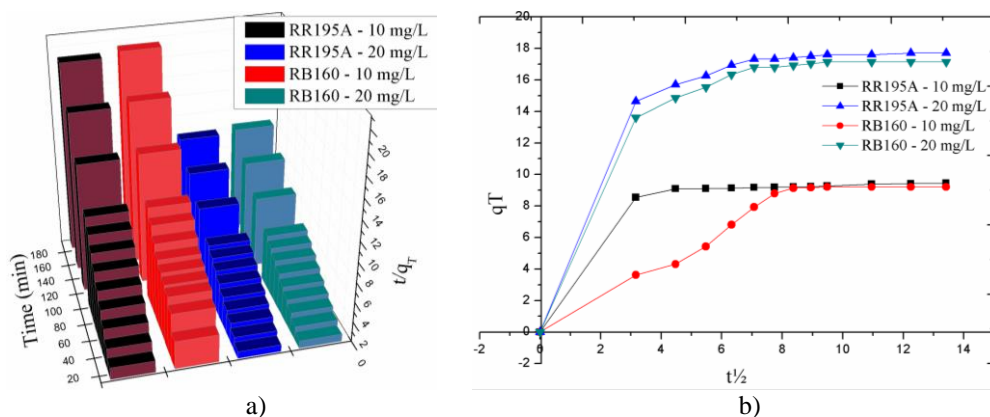


Fig. 8 a) Pseudo-second order kinetics b) Intra-particle diffusion

Table.3. Adsorption kinetic pattern

	RR195A		RB160	
	10 mg/L	20 mg/L	10 mg/L	20 mg/L
$q_{equ}(exp)(mg/g)$	9.45	17.70	9.21	17.14
<i>Pseudo first order reaction</i>				
$q_{equ}(mg/g)$	1.499	5.432	5.75	8.77
$K_1 (min^{-1})$	0.025	0.039	0.030	0.055
R^2	0.758	0.886	0.432	0.952
<i>Pseudo second order reaction</i>				
$q_{equ}(mg/g)$	9.524	18.18	10.20	17.544
$K_2 (min^{-1})$	0.06	0.02	0.0067	0.0210
R^2	0.999	0.999	0.980	0.999
<i>Intra-particle Diffusion</i>				
K_p	0.441	0.525	0.831	0.553

4.4 Isotherm pattern

A pattern of isotherm studies can be done to predict the mechanism of nanocomposite and the adsorbate. The isotherms studies were conducted by using the optimised values for each of the dye attempted.

Langmuir model:

Homogenous monolayer surface interaction can be expressed as [18]

$$\frac{C_{equ}}{q_{equ}} = \left(\frac{1}{Q_0}\right) \left(\frac{1}{b}\right) + \left(\frac{1}{Q_0}\right) C_{equ} \quad (7)$$

where q_{equ} = the amount of dye adsorbed at equi. ; C_{equ} = the equi. conc. of adsorbate (mg/L); Q_0 = Langmuir constant; b = constant relating adsorption energy. The slope and intercept can be obtained from $\frac{C_{equ}}{q_{equ}}$ Vs C_{equ} plot (Fig. 9a & b) for both the dyes taken.

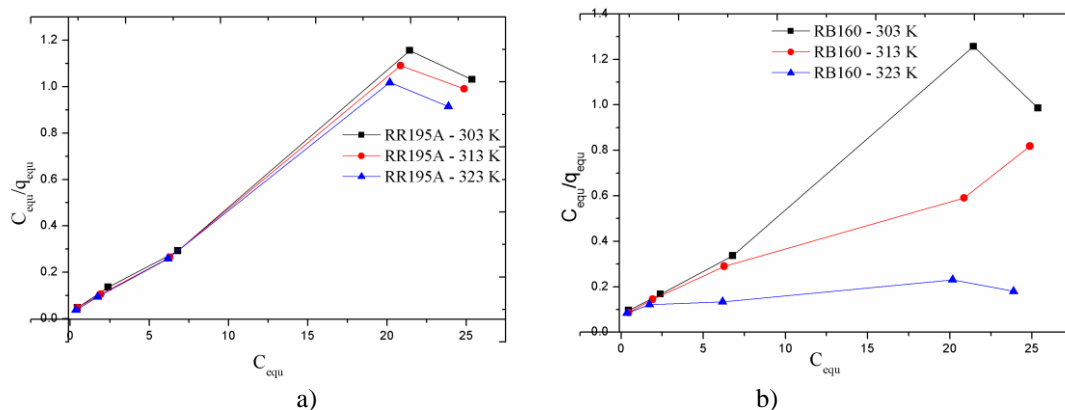


Fig.9. Linear plot of Langmuir isotherm a) RR195A & b) RB160

On comparison, (Table 4) R^2 value assures to best fit the Langmuir isotherm than Freundlich isotherm model. The better fit conveys that the adsorption of RR195A and RB160 class of dyes onto *PNS*-nanocomposite involve in the monolayer adsorption process. The larger size molecule of dyes sticks to the number of active sites of the magnetic natured nanocomposite, hence it was expected to be monolayer and the result obtained also justifies it [9]. As displayed in Fig. 9a, the adsorption mechanism of RR195A onto *PNS*-nanocomposite. Fig. 9b, specifies the adsorption of RB160 by *PNS*-nanocomposite with its linearity and portrays the better fit than another isotherm model. Hence from the values of Fig. 9 and Table 3, it can be well described that the working mechanism of *PNS*-nanocomposite onto the adsorbates.

Table.4. Isotherm postulates

RR195A	Langmuir			Freundlich		
	Q_0	B	R^2	N	K_{Fr}	R^2
303 K	22.727	1.630	0.96	5.128	12.85	0.748
313 K	23.256	1.792	0.956	5.155	13.304	0.721
323 K	23.810	1.750	0.960	5.155	13.803	0.765
RB160						
303 K	22.222	1.071	0.928	4.310	11.24	0.699
313 K	29.412	0.557	0.998	3.195	11.27	0.919
323 K	62.500	0.211	0.876	5.155	13.80	0.765

A dimensionless parameter, separation factor (R_{se}) and the equation is given below:

$$R_{se} = \frac{1}{1+bC_i} \quad (8)$$

where C_i = the initial conc. of dye and b = Langmuir energy constant. The R_{se} values convey the feasibility of the reaction. Accordingly, the R_{se} value ranges from 0.011-0.280 for RR195A and 0.023 – 0.138 as mentioned in the below Table 5 which represents a favourable process of adsorption between the prepared adsorbent and dye molecule adsorbate [14].

Table 5. Separation factor determination

	Separation factor R_{se}					
	B	10 mg/L	20 mg/L	30 mg/L	40 mg/L	50 mg/L
RR195A						
303 K	1.62963	0.058	0.030	0.020	0.015	0.012
313 K	1.79167	0.053	0.027	0.018	0.014	0.011
323 K	1.75	0.054	0.028	0.019	0.014	0.011
RB160						
303 K	1.07	0.085	0.045	0.030	0.023	0.018
313 K	0.55	0.154	0.083	0.057	0.043	0.035
323 K	0.313	0.242	0.138	0.096	0.074	0.060

Freundlich isotherm: the linearised form:

$$\log q_{equ} = \log K_{Fr} + \left(\frac{1}{n}\right) \log C_{equ} \quad (9)$$

where K_{Fr} = the constant relating adsorption capacitance and n = the heterogeneity factor. The empirical constants reflect the adsorptions capacity and the heterogeneity factor [10]. By applying the equation 5, the results obtained were tabulated in Table 3 indicating the unfavourable nature. This unfavourable intellect was due to the larger size of adsorbate, which cannot construct multilayer interaction onto the surface of the adsorbent. Hence from this, it can be concluded that the adsorption mechanism of adsorbent with both the adsorbates does not possess heterogeneity and multilayer interaction in it.

4.5 Thermodynamic pattern

Thermodynamic pattern values deduce the evaluation process of the reaction in the form of successive feasibility and mobility of the reaction between adsorbent and adsorbate. In the present work, thermodynamic macroscopic parameters: entropy change, enthalpy change and free energy [17]. These variables were determined at three different temperatures (303 K - 323 K). The calculations were made by the equations mentioned below

$$\Delta G_1 = -RT \ln K_i \quad (10)$$

$$\Delta S_1 = (\Delta H_1 - \Delta G_1)/T \quad (11)$$

The results of adsorption of RR195A and RB160 onto the adsorbent and their thermodynamic property were calculated by using equation (10 & 11) and tabulated in Table. 6. It indicates the positive values of entropy (ΔS_1) and enthalpy (ΔH_1) and the negative free energy (ΔG_1). These values show that the executed processes are spontaneous in nature and profitably endothermic [18]. These values portray the thermodynamic adsorption process between *PNS*-nanocomposite and reactive dyes were probably temperature dependent. These results also convey that at all nominal temperatures the synthesised *PNS*-nanocomposite was active and its uptake nature was incredible.

Table 6. Thermodynamic pattern

	ΔS_1	ΔH_1	ΔG_1^0 (KJ/mol)		
			303 K	313 K	323 K
RR195A					
10 mg/L	55.80357	9328.308	-7580.17	-8138.21	-8696.24
20 mg/L	66.07136	14940.26	-5079.36	-5740.08	-6400.79
30 mg/L	27.07038	5078.191	-3124.14	-3394.84	-3665.54
RB160					
10 mg/L	37.26335	5361.699	-5929.1	-6301.73	-6674.36
20 mg/L	57.70747	13003.1	-4482.27	-5059.34	-5636.42
30 mg/L	131.6938	37429.63	-2473.58	-3790.52	-5107.46

5. Conclusions

This research study proposed the synthesis of *PNS*-nanocomposite using simplified co-precipitation method from *PNS*-AC. *PNS*-nanocomposite is a low cost and affordable adsorbent for the treatment of wastewater clean-up process. The microporous and mesoporous structure of *PNS*-nanocomposite is a better compliment from the results of BET surface area portraying their vast availability of active pores. The VSM data results (M_s and M_r) project the magnetic capability of the adsorbent. Raman spectra better confirms the existence of functional groups (Fe-O & Fe-OH) with the peaks resulted indicating the bonding intruded by iron oxide onto the surface of AC. The p-XRD justifies the formation of magnetite particles onto *PNS*-AC surface and it also describes their crystallinity nature and was better confirmed by SAED pattern by the availability of bright dots. HR-TEM analysis pictured the pseudo-ball shape of iron oxide particles onto the precursor and the size range (3- 7 nm) justifying the result of Scherrer's equation.

The mobility and reactants dependency of the reaction process was better described by the best fit of pseudo-second order kinetic model. The better fit of monolayer Langmuir adsorption isotherm conveys the reaction involved by the molecules of dyes onto the surface of the adsorbent and the maximum adsorption capacity of RR195A - 23.8 mg/g and RB160 - 62.5 mg/g. The adsorbents temperature dependency was well confirmed by the thermodynamic parameter values. The negative ΔG_1 , positive $-\Delta S_1$ & ΔH_1 also explains the spontaneous and endothermic nature of the executed reaction process. On the whole, the applications and results of various studies executed on the adsorbent portray that the synthesised *PNS*-nanocomposite will be an approachable and affordable adsorbent in the uptake of synthetic dyes from wastewater.

Acknowledgement

We are grateful to SAIF- IITM, STIC-CUSAT and Alagappa university, Karaikudi for their support in providing the accurate measurements through VSM, HR-TEM and p-XRD analysis results respectively.

References

- [1] R. Elmoubarki, F.Z. Mahjoubi, H. Tounsadi, J. Moustadraf, M. Abdennouri, A. Zouhri, A. El Albani, N. Barka, *Water Resources and Industry* **9**, 16 (2015).
- [2] E.T. Abdel Salam, K.M. Abou El-Nour, A.A. Awad, A.S. Orabi, *Arabian Journal of Chemistry*, <http://dx.doi.org/10.1016/j.arabjc.2017.02.005>, (2015).
- [3] Beatriz Acevedo, Carmen Barriocanal, *RSC advances*, **1**, 1 (2013).
- [4] F. Marrakchi, Muthanna J. Ahmed, W.A. Khanday, M. Asif, B.H. Hameed, *Journal of the Taiwan Institute of Chemical Engineers* **71**, 47 (2017).
- [5] M. Srinivas Kini, M. B. Saidutta and V. Ramachandra Murty, *International Journal of Chemical Engineering*, **2014**(306519),1 (2014).
- [6] G. Somaia Mohammad, M. Sahar Ahmed, M. Abdel Fattah Badawi and D.S. El-Desouki, *Journal of Applied Life Sciences International* **3**, 77(2015).
- [7] Osman Gulnaz, Aysenur Kaya, SadikDincer, *Journal of Hazardous Materials B* **134**, 190 (2006).
- [8] ChahrazedDjilani, RachindaZaghdoudi, FaycalDjazi, BachirBoucheKima, AbdelazizLallam, Ali Modarressi, Marek Rogalski, *Journal of the Taiwan Institute of Chemical Engineers*, **53**, 112 (2015).
- [9] Ruhul Amin Reza, M. Ahmaruzzaman, *RSC Advances* 1039 (2013).
- [10] Ageetha Vanaamudan, Padmaja P. Sudhakar, *Journal of the Taiwan Institute of Chemical Engineers*, **55**, 145 (2015).
- [11] K. Muthukumar and S. Sophie Beulah, *Procedia Environmental Sciences*, **4**, 266 (2011).
- [12] H. Jae Kwon, D. Lee Wilson, R. Sammynaiken, *Synthetic Metals* **197**, 8 (2014).
- [13] ArunaJyothi Kora, Sashidhar Rao Beedu and Arunachalam Jayaraman, *Organic and*

Medicinal Chemistry Letters **2** (2012) .

[14] P. Diana Vargas, Liliana Giraldo Gutierrez and Juan Carlos Moreno-Pirajan, Adsorption Science & Technology **31**, 845 (2013).

[15] Hong Yang, Qiyang Feng, Journal of Hazardous Materials **180**, 160 (2010).

[16] NavishKataria, V.K. Garg, Journal of Environmental Chemical Engineering, **35** (2017).

[17] NafisehMansouriieh and Mahmoud Reza Sohrabi, Indian Journal of Chemical Technology, **24**, 383 (2017).

[18] B.B. Zhang, J.C.Xu, P.H.Xin, Y.B.Han, B.Hong, H.X.Jin, D.F.Jin, X.L.Peng, J.Li, J. Gong, H.L.Ge, Z.W.Zhu, X.Q.Wang, Journal of Solid State Chemistry, **221**, 302 (2015).